PCCP

Exciton-vibrational dynamics induces efficient self-trapping in a substituted nanoring

Journal:	*Physical Chemistry Chemical Physics*
Manuscript ID	CP-ART-07-2022-003162.R1
Article Type:	Paper
Date Submitted by the Author:	20-Sep-2022

Complete List of Authors:	Alfonso-Hernandez, Laura; Universidad Nacional de Quilmes, Science and Technology Freixas Lemus, Victor; Universidad Nacional de Quilmes, Science and Technology Rodriguez-Hernandez, Beatriz; Universidad Nacional de Quilmes, Science and Technology Tretiak, Sergei; Los Alamos National Laboratory, Theoretical Division Fernandez-Alberti, Sebastian; Universidad Nacional de Quilmes, Science and Technology Oldani, A; Universidad Nacional de Quilmes, Science and Technology

Exciton-vibrational dynamics induces efficient self-trapping in a substituted nanoring

Laura Alfonso Hernandez[1], Victor M. Freixas[1], Beatriz Rodriguez-Hernandez[1], Sergei Tretiak[2], Sebastian Fernandez-Alberti[1*]and Nicolas Oldani[1]

[1]Departamento de Ciencia Tecnologia, Universidad Nacional de Quilmes/CONICET, B1876BXD Bernal, Argentina
[2]Theoretical Division and Center for Integrated Nanotechnologies, Los Alamos National Laboratory, Los Alamos, New Mexico 87545, USA

*corresponding author: sfalberti@gmail.com

ABSTRACT

Cycloparaphenylenes, being the smallest segments of carbon nanotubes, have emerged as prototypes of the simplest carbon nanohoops. Their unique structure-dynamics-optical properties relationships have motivated a wide variety of synthesis of new related nanohoop species. Studies of how chemical changes, introduced in these new materials, lead to systems with new structural, dynamics and optical properties, expand their functionalities for optoelectronics applications. Herein, we study the effect that conjugation extension of a cycloparaphenylene through the introduction of a satellite tetraphenyl substitution, has on its structural and dynamics properties. Our non-adiabatic excited state molecular dynamics simulations suggest that this substitution accelerates the electronic relaxation from the high-energy band to the lowest excited state. This is partially due to efficient conjugation achieved between specific phenyl units as introduced by the tetraphenyl substitution. We observe a particular exciton redistribution during relaxation, in which the tetraphenyl substitution plays a significant role. As a result, an efficient inter-band energy transfer takes place. Besides, the observed phonon-exciton interplay induces a significant exciton self-trapping. Our results, encourage and guide the future studies of new phenyl substitutions in carbon nanorings with desired optoelectronic properties.

I. INTRODUCTION

Cycloparaphenylenes ([n]CPPs) are cyclic conjugated structures comprised of n sequential phenyl rings bonded covalently at the *para* position, representing the smallest unit cycle of an armchair nanotube. Since their initial synthesis[1–3], they attracted the attention of the scientific community due to their unique structural properties that combine bending and torsional strains, disorder and steric hindrances[4–6]. These structural properties affect the π-orbital overlaps between phenylene units and conjugation lengths. After photoexcitation, [n]CPPs experience dynamical changes such as planarization of the chain, changes in their bond length alternation, exciton intramolecular spatial redistribution, and self trapping[6,7,5]. These behaviours in turn impact their electronic and optical properties[8–16]. [n]CPPs are highly fluorescent compounds whose quantum yield significantly increases with n[9,17,12,10]. In contrast to the red shifts observed in their linear counterparts (oligophenylenes), [n]CPPs experience fluorescence blueshift with increasing n. Moreover, [n]CPPs absorption spectra results are virtually independent of n, in contrast with pronounced redshifts observed while increasing n in linear oligophenylenes[18]. These peculiar size-dependent optoelectronic properties make [n]CPPs attractive materials for implementation as organic semiconductors, light harvesters and sensors[19].

Unique diversity of photophysical properties of [n]CPPs is stemming from the synthesis of a large variety of related nanohoops[20] frequently combined with other building blocks[21–26], with inserted acene units, like naphthalene, anthracene, and tetracene[27–29], nanobelts[30–32], nanocages[33], interlinked and covalently connected CPP units and knots[34], to name a few. Experimental and modelling studies of these systems reveal that unique structure-dynamics-optical properties relationships of carbon nanohoops can be subjected to tuning, achieving desired optoelectronic properties as required in a broad scope of next-generation technologies in the field of solid-state nanomaterials, biologically relevant fluorophores, and sensors, among others[19,35].

Establishing detailed relationships of [n]CPP structural properties with their optical and electronic features requires an atomistic description of the structural and dynamical changes that accompany the internal conversion process that takes place for electronically excited states. This involves the electronic and vibrational energy relaxation and redistribution of energy among coupled electronic excited states. Non-adiabatic excited state molecular dynamics simulation is a powerful theoretical framework to address these issues, this is the case of NEWTON-X[36,37], SHARC[38,39] (surface hopping including arbitrary couplings), PYXAID (PYthon eXtension for Ab Initio Dynamics),[40, 41] AIMS(ab initio multiple spawning)[42,43], and NEXMD (Non-adiabatic EXcited-states Molecular Dynamics)[44, 45] have been applied to a wide variety of organic materials and photophysical and photochemical processes[46–60]. These methods have been previously applied to simulate the photoinduced electronic energy relaxation and redistribution in CPPs and related nanohoops[61,62]. Particularly, the NEXMD (Nonadiabatic EXcited-state Molecular Dynamics) software package[44] have been extensively applied to a variety of CPPs[8,5], and related nanohoops[63,26], nanobelts[64] and nanocages[65]. These previous investigations have revealed that structural modifications introduced in CPPs by various substitutions and insertions induce changes in the relative efficiency of the internal conversion process

involving dynamical changes of the structures such the local planarization of the chain and concomitant changes in the specific exciton spatial localization (self-trapping)[53] occurring during the excited-state dynamics.

In the present work, we access the effect that extension of conjugation on [12]CPP, through the introduction of a satellite tetraphenyl substitution (denoted as T-[12]CPP), has on its structural and dynamical properties. This system has been synthetized and characterized by the group of Jasti[66] as a preliminary precursor to the synthesis of an ultrashort carbon nanotube. Particularly, photoexcitation at the ~240nm high energy band, ascribed to the tetraphenyl substitution, allows to analyse the details of the subsequent intramolecular energy relaxation and redistribution of the nanoring.

The paper is organized as follows: In Section II we present a brief overview of the computational approach, methods used to analyse transient changes in the electronic transition density and the interplay between structural changes and exciton self-trapping. We discuss our results in Section III, and summarize our findings in Section IV.

II. COMPUTATIONAL METHODS

A. NEXMD background. The NEXMD package has been developed to simulate non-adiabatic excited-state molecular dynamics in large conjugated multi-chromophore systems involving multiple coupled electronic excited states. It combines mixed quantum-classical algorithms[67,68] with "on the fly" analytical calculations of excited state energies, gradients and non-adiabatic coupling terms at the configuration interaction singles (CIS) level combined with the semiempirical Hamiltonian models. Across several non-adiabatic algorithms implemented in NEXMD, here we use trajectory surface hopping approach[67,68], where nuclei are propagated classically and the electronic wave function $\psi(t) = \sum_\alpha c_\alpha(t)\phi_\alpha$ is propagated quantum-mechanically in the basis of adiabatic electronic states with wavefunctions ϕ_α:

$$i\hbar\dot{c}_\alpha(t) = c_\alpha(t)E_\alpha - i\hbar\sum_\beta c_\beta(t)\boldsymbol{v}\cdot\boldsymbol{d}_{\alpha\beta} \quad (1)$$

Where $E_\alpha$is the energy of the α^{th} electronic excited state, $\boldsymbol{v}$ are the velocities associated with nuclear coordinates $\boldsymbol{r}$ and $\boldsymbol{d}_{\alpha\beta}$ are the non-adiabatic derivative coupling vectors (NACR) defined as $\boldsymbol{d}_{\alpha\beta} = \langle\phi_\alpha|\nabla_{\boldsymbol{r}}\phi_\beta\rangle$. More details related to the NEXMD approach, implementation, advantages and testing parameters can be found in our previous works[53, 44,69].

B. Analyses of transient spatial exciton redistribution. The exciton transient spatial localization is monitored by calculating the evolution in time of transition density matrices expressed in atomic orbital (AO) basis: $(\rho^{0\alpha})_{ij} = \langle\phi_\alpha|c_i^\dagger c_j|\phi_0\rangle$[70], with ϕ_0 and ϕ_α being the wavefunctions corresponding to the adiabatic ground- and excited- states, respectively, $c_i^\dagger$ and c_j are the respective creation and annihilation operators acting over AO i and j[53]. The diagonal element $(\rho^{0\alpha})_{ii}$ represents the change in the net charge of the electronic density on AO i during a transition from the ground- to the adiabatic excited-state α. The fraction of $\rho^{0\alpha}$ localized on a selected or set of x selected phenylene units can be calculated as

$$\delta_x = \left(\rho^{0\alpha}\right)_x^2 = \frac{\sum_{i \in x}(\rho^{0\alpha})_{ii}^2}{\sum_i (\rho^{0\alpha})_{ii}^2}. \qquad (2)$$

with $\sum_x^n \delta_x = 1$ and the extent of the exciton self-trapping in terms of the number of phenylene units across which it is spread, can be measured using the participation number[71,72]

$$PN_n(t) = \left[\sum_x^n (\delta_x)^2\right]^{-1} \qquad (3)$$

with n being the total number of phenylene units included. Values of $PN_n(t) \approx 1$ indicate a complete localization of $\rho^{g\alpha}(t)$ on the phenylene or set of phenylenes x, while values of $PN_n(t) \approx$ n indicate the fully delocalized case when $\rho^{g\alpha}(t)$ spread equally among rings.

B. Transition density fluxes. The effective energy transfer between phenylene units can be monitored by using the transition density flux analysis[73,74].

At each time interval Δt throughout the NEXMD simulations, $\Delta\delta_x(t) = \delta_x(t) - \delta_x(t - \Delta t)$ is calculated by the flow matrix F(t) with null diagonal elements and off-diagonal elements $f_{xy}(t)$ containing the amount of $\delta_x(t)$ transferred between units x and y. The chromophore units are classified as donors (D) and acceptors (A) for $\Delta\delta_x(t) < 0$ and $\Delta\delta_x(t) > 0$, respectively. Considering only the effective $\delta_x(t)$ flow from D to A, the total transition density fraction exchanged between the units during time Δt is calculated as

$$\Delta\delta_{total}(\mathrm{t}) = \sum_{x \in D} \left|\Delta\delta_x(\mathrm{t})\right| = \sum_{y \in A} \Delta\delta_y(\mathrm{t}) \qquad (4)$$

and elements $f_{\mathrm{yx}}(t)$ are evaluated as

$$f_{xy}(t) = -f_{yx}(t)$$

$$= \begin{cases} \frac{|\Delta\delta_x(t)|\Delta\delta_y(t)}{} & \mathrm{x} \in \mathrm{D}, \mathrm{y} \in \mathrm{A} \\ 0 & x, \mathrm{y} \in \mathrm{D} \text{ or } \mathrm{x,y} \in \mathrm{A} \end{cases} \qquad (5)$$

A detailed derivation of eq (5) can be found elsewhere[73].

D. Representative non-adiabatic derivative coupling vectors. The Singular Value Decomposition (SVD) technique can be used to identify representative vectors of non-adiabatic derivative couplings $\boldsymbol{d}_{\alpha\beta}$ for the ensemble of NEXMD simulations. For this purpose, a matrix **A** of dimension $3N \times K$ is built, with N being the number of nuclear degrees of freedom and K is the number of NEXMD simulations featuring a selected effective $S_\alpha \rightarrow S_\beta$ transition (i.e., a hop). An effective $S_\alpha \rightarrow S_\beta$ transition is defined as the last $S_\alpha \rightarrow S_\beta$ transition without subsequent $S_\beta \rightarrow S_\alpha$ back-hopping during the rest of the simulation. The columns of **A** contain the $\boldsymbol{d}_{\alpha\beta}$ at the moment of effective $S_\alpha \rightarrow S_\beta$ transition in each of the K NEXMD trajectories. Then, SVD is performed as

$$\mathbf{A} = \mathbf{U} \cdot \mathbf{W} \cdot \mathbf{V}^{T} \quad (6)$$

where **U** is a 3*N*x*K* column-orthogonal matrix, and **V** and **W** are *K*x*K* diagonal and orthogonal matrices, respectively. We denote $\boldsymbol{d}_{\alpha\beta}^{SVD,i}$ as the i^{th} column of the matrix **U** with the associated largest value of w_i. The $\boldsymbol{d}_{\alpha\beta}^{SVD,k}$ vector or vectors with the largest w_k can then be considered as a representative of the ensemble of $\boldsymbol{d}_{\alpha\beta}$ collected from the different NEXMD simulations.

E. Computational details. The photoexcitation and subsequent electronic relaxation of T-[12]CPP and [12]CPP (see **Figure 1(a)** for molecular representation) have been simulated using the NEXMD package using the semiempirical AM1 Hamiltonian model[75]. AM1 in combination with CIS has been previously validated for [n]CPP and related nanorings with respect to DFT calculations with 6-31G* basis set and the Coulomb-attenuated hybrid B3LYP (CAM-B3LYP) functional[8]. Generally, AM1/CIS approach provide a consistent red-shifts of transition energies by about 0.3 eV for nanorings in comparison with experiment or high-level theories. The NEXMD simulations were performed at a constant energy. Initial conditions were collected from 1 ns-long equilibrated ground state molecular dynamics simulation performed for each system at room temperature (T=300 K) with the Langevin thermostat and friction coefficient $\gamma = 20.0\, ps^{-1}$. Absorption spectra were calculated by collecting vertical transition energies and oscillator strengths obtained from the 1000 configurations collected during these equilibrated ground state simulations. For each system, 400 NEXMD trajectories were calculated. These trajectories were started using coordinates and momenta collected from the corresponded previous equilibrated ground state simulations. For each NEXMD trajectory, the initial excited state is then selected according to a Frank-Condon window given by $g_\alpha(\boldsymbol{r}, \boldsymbol{R}) = \exp\left[-T^2(E_{laser} - \Omega_\alpha)^2\right]$, where E_{laser} represents the energy of a laser pulse centred at the maximum of the high energy band, and is localized at 260 and 255 nm for T-[12]CPP and [12]CPP, respectively (see **Figure 1(c, d)**). Ω_{alpha} is the adiabatic energy of the α^{th} state**.** A Gaussian laser pulse, $f(t) = \exp\left(-t^2/2T^2\right)$, with $T = 42.5$ fs, corresponding to a FWHM (Full Width at Half Maximum) of 100 fs, has been used. For each NEXMD simulation, the relative values of $g_\alpha(\boldsymbol{r}, \boldsymbol{R})$, weighted by the oscillator strengths of each α state, have been applied to select its initial excited state. Classical time steps of 0.5 and 0.1 fs have been used for nuclei propagation in the ground state and NEXMD trajectories, respectively. Additionally, a quantum time step of 0.025 fs has been selected to propagate the electronic coefficients during NEXMD trajectories. Specific treatments of decoherence[76] and trivial unavoided crossings[77] have been utilized in these simulations as well as default options.

III. RESULTS AND DISCUSION

Nonadiabatic excited state molecular dynamics simulations have been performed for [12]CPP and T-[12]CPP systems. T-[12]CPP is composed of [12]CPP with a tetraphenyl substitution formed by four additional satellite phenyl units, as shown in **Figure 1(a)**. In agreement with experimental results[66], the absorption spectra of both molecules, shown in **Figures 1(b-c)**, do not differ significantly except by the presence of low-intensity absorption states at the energy gap between bands. The broadening used to construct the absorption spectra histograms was 0.15 eV. Two absorption bands can be observed separated by ~1.6 eV, either for [12]CPP and T-[12]CPP. This results is in reasonable agreement with experimental the energy gap of ~1.4 eV[66]. As it has been previously pointed out[8], transition energies for excited states for [n]CPP and related nanohoops are red shifted by ~0.3 eV compared to experiments. Nevertheless, the shift. is consistent for this molecular family and the trends observed can be trusted. During the process of energy relaxation and redistribution more important than the relative absorption intensity between peaks is the energy gap between states. The high-energy band of T-[12]CPP has been previously assigned mainly to excitations involving the tetraphenyl substitution[66]. This is confirmed in **Figure S1**, where the spatial localization of the electronic transition density, evaluated for [12]CPP and T-[12]CPP, are shown for selected sets of electronic excited states. We can observe that the high energy band is composed of excited states with different degree of delocalization between the satellite phenyl units and the nanoring. Besides, states in between the two absorption bands, i.e., S_{28}-S_{31}, are also partially localized at the tetraphenyl substitution.

The main difference between both absorption spectra is a reduced density of excited states between ~3.6 and 4.4 eV for the unsubstituted system. As shown un **Figure 1(d)**, the density of states within this energy gap is higher for T-[12]CPP with respect to [12]CPP. This feature is expected to impact the internal conversion to S_1 after photoexcitation at the high-energy band. The evolution of state populations obtained from the NEXMD simulations of [12]CPP and T-[12]CPP is shown in **Figure 2**. Overall, we can observe a similar behaviour in both systems. That is, after an ultrafast energy relaxation across a dense manifold of high-energy states, a long-lived state appears. This state is separated from lower energy states by large energy gaps and slows down the relaxation. While the populations of long-lived states reach the maximum at about the same time for [12]CPP and T-[12]CPP, a faster subsequent relaxation of this state (S_{33}) is observed during the dynamics of T-[12]CPP compared to the respective long-lived state (S_{25}) of [12]CPP. As a consequence the net internal conversion rate is faster in T-[12]CPP.

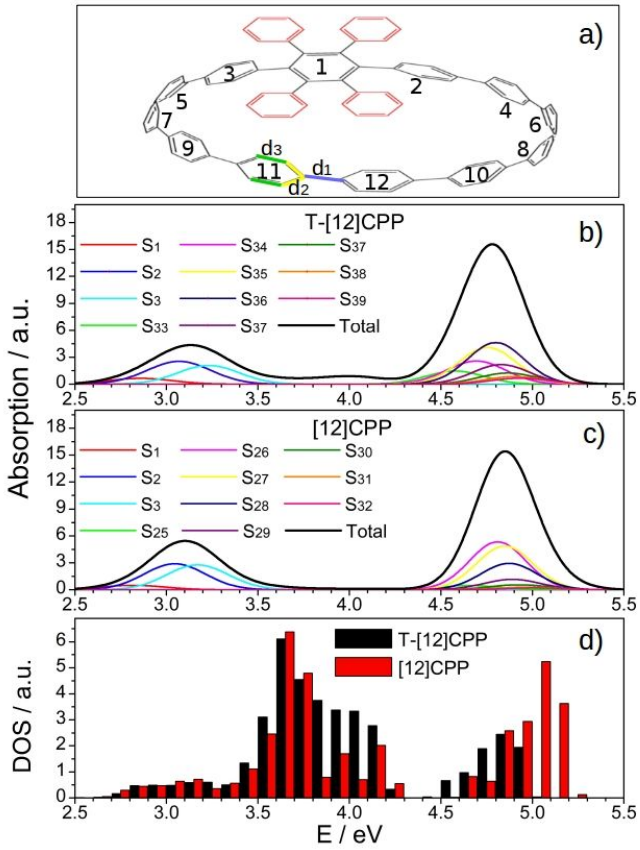

Figure 1. (a) Schematic representation of the tetraphenyl-substituted [12]CPP (T-[12]CPP). The four satellite phenyl units are shown in red and bonds entering bond length alternation (BLA) parameter are indicated. The phenylene units are numbered according to their distance with respect to the tetraphenyl insertion; (b) and (c) Simulated absorption spectra of [12]CPP and T-[12]CPP, respectively, showing the individual contributions of selected excited states; (d) Contribution of the different adiabatic electronic states to the density of states within energy intervals of 0.1 eV, calculated at the minimum energy configuration of each system

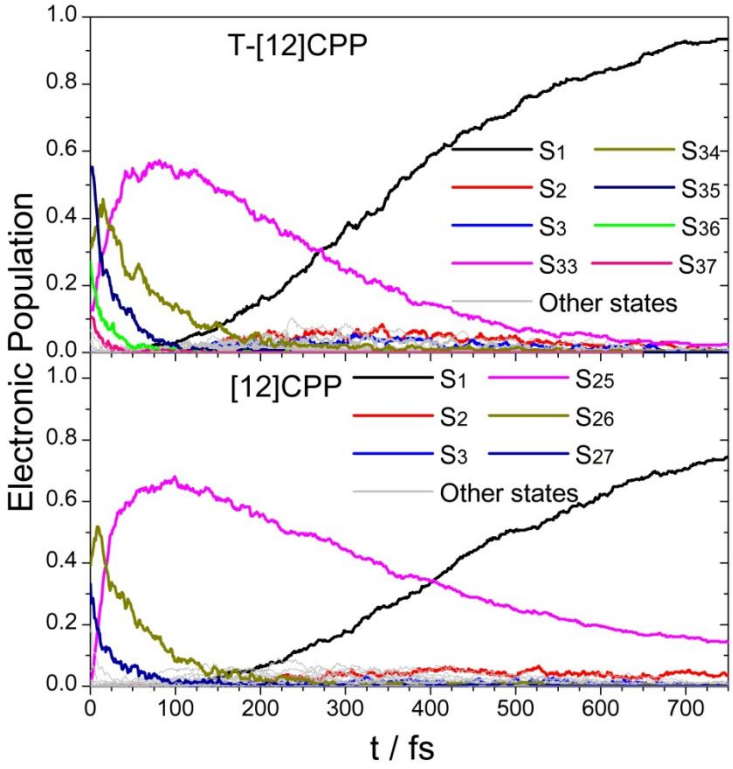

Figure 2. Evolution of average populations of relevant electronic states with time when simulation trajectory ensemble of T-[12]CPP and [12]CPP.

The faster relaxation of T-[12]CPP is associated with the presence of higher density of states in the energy gap that separates the two main absorption bands in T-[12]CPP, as shown in **Figure 1(d)**. The electronic states within this energy gap of T-[12]CPP correspond to the range of states [S_6:S_{32}]. The excited state distribution of δ_{star} (i.e., the fraction of transition density localized on the star composed by the four satellite phenyl units and the phenylene unit numbered as 1, see **Figure 1(a)**) during excited state dynamics for each state, is presented in **Figure 3(a)**. The exciton localization in the star is circumscribed to only a few states in the range [S_{24}:S_{32}] and the S_{33} long-lived state. A similar spatial localization of the transition density of these states increases the coupling between them and accelerates the electronic relaxation. **Figures 3(b,c)** display the distribution of fractions electronic transitions (χ), or hops, from the long-lived state to the subsequent states which are lower in energy. There is a larger number of pathways involving different direct transitions from the long-lived state to lower energy states in T-[12]CPP compared to that in [12]CPP. We can observe larger values of delay times, defined as t-t_{hop}, i.e., the relative time with respect to the hopping time t_{hop}, from the long-lived S_{25} state during [12]CPP simulations with respect to the corresponding delay times from the S_{33} during T-[12]CPP simulations. This indicates a more passage of the corresponding energy gap between absorption bands by the presence of the tetraphenyl substitution. This substitution introduces new states, with significant values of δ_{star}, that facilitate the non-radiative relaxation through multiple alternative pathways.

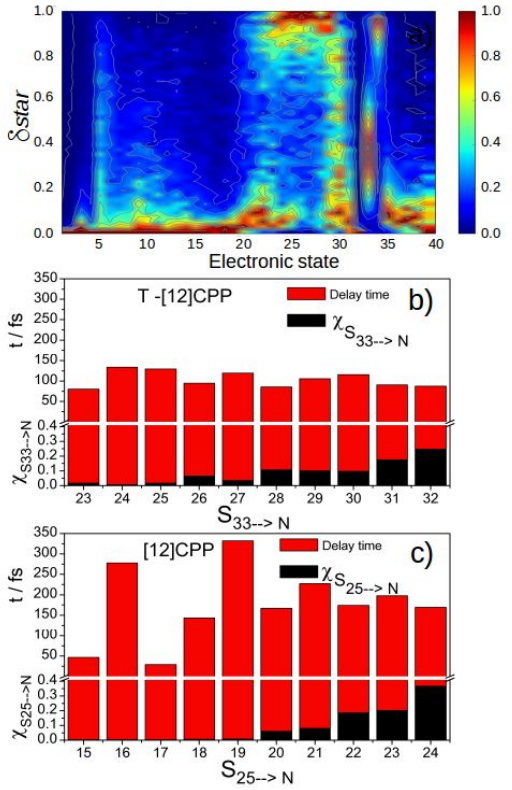

Figure 3. (a) Contour plot of the probability density of δ_{star}, i.e., the fraction of transition density localized on the star composed of the four satellite phenyl units and the phenylene unit numbered as 1 (see **Figure 1(a)**), obtained from collected values at any time during excited state dynamics for each state. The color bar corresponds to the fraction of the corresponding values of δ_{star} at each electronic state. (b, c) Fraction of electronic transitions (χ) from the long-lived S_{33} and S_{25} states to the subsequent lower in energy states (black blocks) and the corresponding delay time (red block), defined as t-t_{hop}, i.e., the relative time with respect to the hopping time from these states to lower-energy states, during T-[12]CPP and [12]CPP simulations respectively.

The insertion of the tetraphenyl units not only modifies the density of states in the energy band gap but also introduces changes in the spatial exciton redistribution dynamics during the internal conversion. Previous studies have shown that this is the case for insertions of acene units[28] and alkyl chains[63]. Here, the insertions modify the final spatial localization of the exciton self-trapping without significant exciton transient delocalizations between the insertion and the rest of the nanoring. This seems not to be the case for T-[12]CPP. **Figure 4(a)** shows the intramolecular exciton spatial redistribution that takes place after photoexcitation of T-[12]CPP at the high energy band. The fractions of electronic transition density, δ_x, localized on different sets x of phenylenes are depicted grouping the phenylene units according to the localization in the star following to the numerical pattern in **Figure 1(a)**. The initial photoexcitation creates an almost complete

exciton delocalization across the entire system. This is followed by an ultrafast transient accumulation of δ_x at the phenylene units of the star and its neighboring phenyls 2 and 3. After the first 100 fs, a pronounced exciton migration from the star region to the rest of the nanoring is observed. As a result, the exciton localizes on the sets of phenylene units far away from the star.

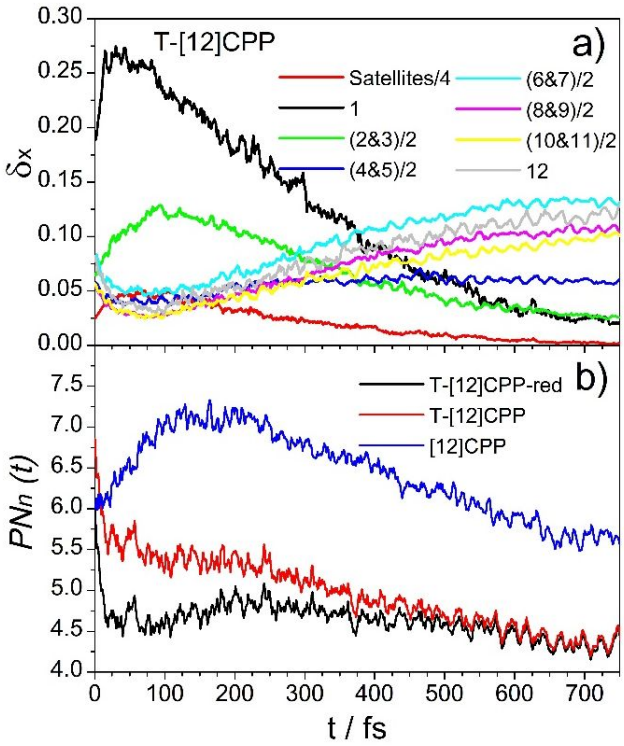

Figure 4 (a) Time-dependence of the average fraction of electronic transition density, δ_x, localized on different sets x of phenyls. The rings are numbered according to Fig. 1(a). (b) Time-dependence of the participation number $PN_n(t)$. T-[12]CPP (in red) represents the calculation of $PN_n(t)$ during the excited state dynamics of T-[12]CPP with renormalization of the diagonal terms of the transition density matrix excluding contributions from the satellite phenylenes**.**

The exciton intra-ring migration described in **Figure 4(a)** leads to an exciton self-trapping in T-[12]CPP distinctly different compared to that in [12]CPP. **Figure 4(b)** shows the variation of the participation number $PN_n(t)$ (see eq. (3)) during the excited state simulations of T-[12]CPP and [12]CPP. More efficient self-trapping is observed for T-[12]CPP. While the relaxed exciton extends over about 6 phenylene unit in [12]CPP, it is confined to only about 4.5 phenyls in T-[12]CPP. The transient exciton delocalization during the first ~200 fs experienced by [12]CPP is not observed by T-[12]CPP, where an almost continuous increase of the exciton lockdown takes place. In order to further analyze the contribution of the satellite phenylene units to this exciton self-trapping, $PN_n(t)$ is recalculated for T-[12]CPP by normalization of the diagonal terms of the transition density matrix $(\rho^{0\alpha})_{ii}$ in order to make $\sum_x^{n_{red}} \delta_x = 1$, with n_{red} involving all phenylene units except

the satellite ones. In this way $PN_n(t)$ varies in the range [1:12] for both [12]CPP and T-[12]CPP. **Figure 4(b)** shows that after ~450fs, that correspond to the time at which $\delta_{\text{satellite}}$, i.e., the fraction of transition density localized on the phenyl satellite units, decreases to values ~1%, both calculations of $PN_n(t)$ for T-[12]CPP agrees. Therefore, the initial spatial exciton redistribution that takes place in T-[12]CPP leads to a more efficient exciton self-trapping involving only phenylene rings localized on the nanohoop.

The specific localization of the exciton self-trapping observed during the excited state dynamics of T-[12]CPP can be associated to concomitant differential changes in its structure with respect to [12]CPP. **Figure 5(a)** and **(b)** shows the evolution in time of the bond length alternation (BLA), calculated as $\text{BLA} = d_1 - d_2 \cdot \frac{2}{3} - d_3 \cdot \frac{1}{3}$, where d_1, d_2, and d_3 are indicated in Fig. 1(a). Smaller values of BLA are associated with better π-conjugation between neighboring phenylene rings and, therefore, evidence an enhancement of the electronic delocalization[78,79,80]. We can observe that the π-conjugation decreases with time for phenylene units localized on the star and its neighbor units (see **Figure 5(a)**). Only BLA values calculated using as central bonds (i.e., the bonds that connect 2-4 and 3-5 phenyls result close to those values obtained for [12]CPP (**Figure 5(b)**). Besides, BLAs related to the connection between phenylene units at long distances of the star have lower values signifying more efficient π-conjugation.

A further inspection of the structural changes in the excited state dynamics induced by the tetraphenyl substitution can be found by analyzing the dihedral angles connecting specific phenyls of T-[12]CPP with respect to the values obtained for [12]CPP. **Figure 5(c)** shows the evolution in time of the average dihedral angles for T-[12]CPP and [12]CPP. Dihedral angles that connect the central phenylene unit 1 of the star (see **Figure 1(a)**) indicate an orthogonal orientation of this units with respect to their neighbors. These dihedral angles do not experience significant planarization during the excited state dynamics. The reason of this can be found in the steric effects between these phenylene units. The other dihedral angles between phenyls localized far from the substitution group feature a more efficient planarization in comparison to that in [12]CPP. This fact explains more pronounced self-trapping on these phenylene units. That is, modifications of π-conjugation during the excited state dynamics, examined through BLA and dihedral angles, lead to a more localized exciton self-trapping with respect to [12]CPP dynamics.

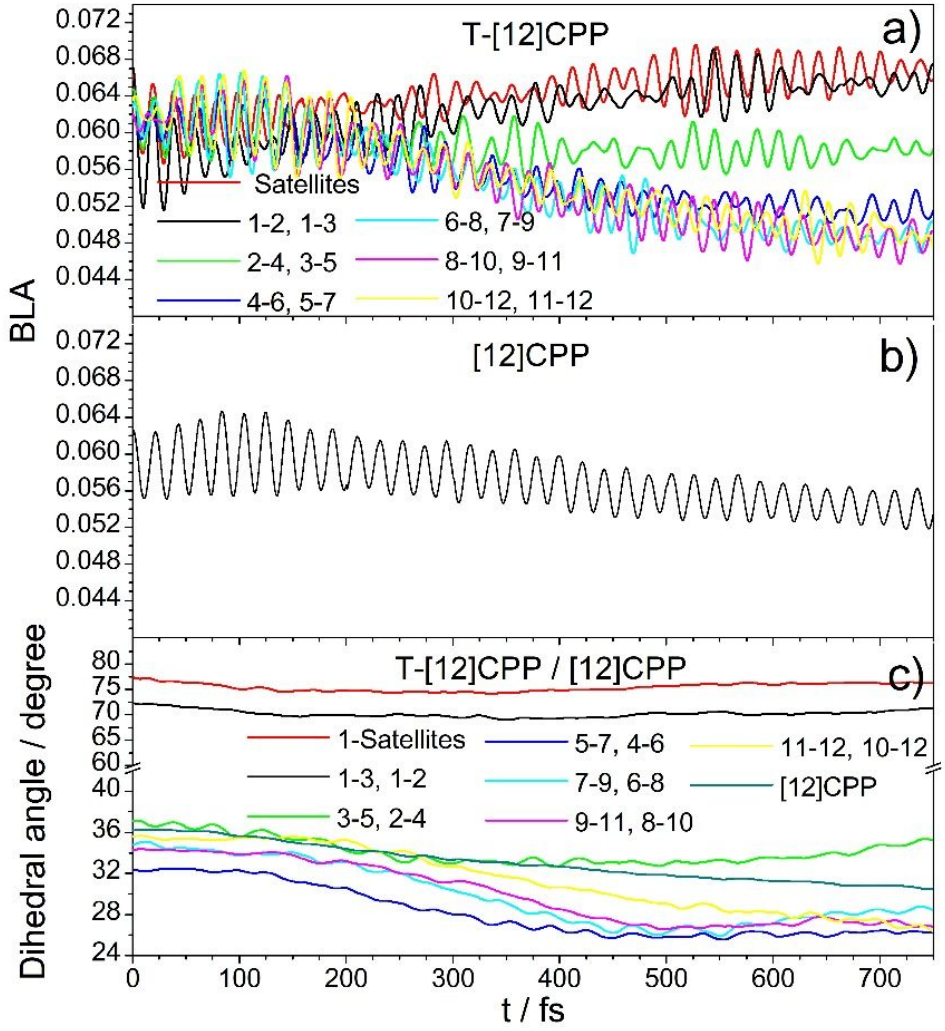

Figure 5. Time-dependence of the average BLA considering central bonds connecting (a) different *i* and *j* phenylene units of T-[12]CPP, (b) all phenylene units of [12]CPP; (c) average dihedral angle connecting specific phenylene units of T-[12]CPP and all phenylene units of [12]CPP. The units are numbered according to Fig. 1(a).

The non-adiabatic coupling vector $\boldsymbol{d}_{\alpha\beta}$ represents the direction of the force acting on the nuclei during the $S_\alpha \rightarrow S_\beta$ transition[81]. Therefore, it describes the direction of vibrational energy transfer during this electronic transition. In T-[12]CPP dynamics, the transition from the long-lived S_{33} to the state lower in energy, i.e. $S_{33} \rightarrow S_{32}$, corresponds to a major vibrational energy redistribution due to the relatively large energy gap $\Delta E_{33\text{-}32}$ = 0.16 eV between these states compared to $\Delta E_{32\text{-}31}$=0.02 eV / $\Delta E_{31\text{-}30}$=0.03 eV / $\Delta E_{30\text{-}29}$=0.02 eV.

Figure 6(a) and **(b)** depicts two representative vectors of the ensemble of $\boldsymbol{d}_{33,32}$, i.e., $\boldsymbol{d}_{33,32}^{SVD,1}$ and $\boldsymbol{d}_{33,32}^{SVD,2}$. Both vectors have the associated equivalent w_k, therefore, the actual $\boldsymbol{d}_{33,32}$ is a superposition of them. We can observe that $\boldsymbol{d}_{33,32}^{SVD,1}$ and $\boldsymbol{d}_{33,32}^{SVD,2}$ correspond to antisymmetric and symmetric motions of phenylene groups at each side of an axis connecting phenyls #1 and #12, respectively. They present a wave-like behavior that can be described in analogy with a particle in a box limited by the tetraphenyl substitution, whose two first stationary solutions correspond to ~$\sin\left(\frac{n\pi}{L}x\right)$ (n=1,2), where L the length of the nanoring chain and x the distance with respect to the tetraphenyl substitution. The fraction of motion involving each phenylene ring in $\boldsymbol{d}_{33,32}^{SVD,1}$ and $\boldsymbol{d}_{33,32}^{SVD,2}$ are shown at the corresponding right side of **Figure 6**. These distributions are related with a stronger final exciton localization and structural distortions shown in **Figures 4-5**.

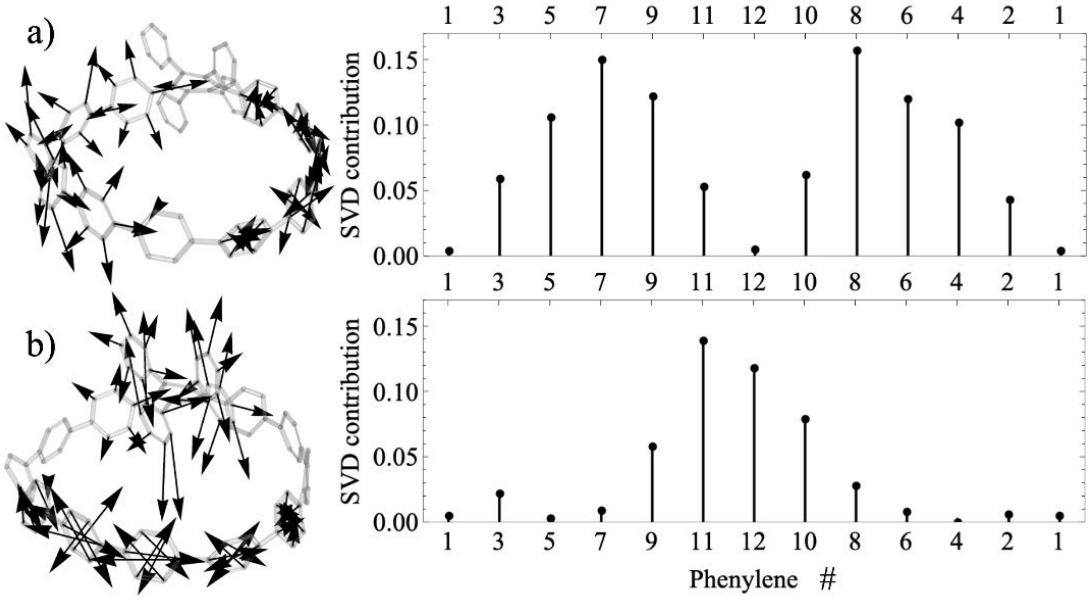

Figure 6. Representation of (a) $\boldsymbol{d}_{33,32}^{SVD,1}$ and $(b)\boldsymbol{d}_{33,32}^{SVD,2}$ during T-[12]CPP nonadiabatic dynamics. The fraction of motion involving each phenyl ring are shown at the corresponding right side panels. The units are numbered according to Fig. 1(a).

The effective energy transfer between phenylene units can also be monitored using the transition density flux, as has been described in Section II.B. **Figure S2** shows these transfers among different ensembles of phenylene units of T-[12]CPP. δ_{star} experiences an initial increase due to the exciton migration from phenyls 10/11/12, 5/4, 6/7, 8/9, as it is indicated by the initial negative flux star→others. These initial fluxes are responsible for the transient accumulation of S_{33} population shown in **Figure 2**. After that, the region of the tetraphenyl substitution back-transfers this energy to the same phenylene units. Except that, no other effective transfers are observed between phenylene units, indicating the static aspect of the final exciton self-trapping.

IV. CONCLUSIONS

The effect that a tetraphenyl substitution has on a nanoring [12]CPP has been investigated using atomistic non-adiabatic excited state molecular dynamics. We simulate and analyze excited state dynamics after photoexcitation at the high-energy band. Long-lived meta-stable states are observed during the relaxation from the high-energy band to the low-energy one. We find that the tetraphenyl substitution increases the density of states in the energy gap between these two main absorption bands of the nanoring. These states have electronic transition densities, and thus excited state wavefunctions, predominantly localized at the tetraphenyl substitution. Compared to the unsubstituted [12]CPP, presence of these states facilitates the electronic relaxation by introducing a larger number of efficient alternative pathways of nonradiative relaxation from the long-lived state to states lower in energy.

Additionally, the insertion of the tetraphenyl modifies electronic and vibrational energy redistributions that differs from the unsubstituted counterpart. Structural rearrangements during excited state dynamics promote a more efficient conjugation in regions distant from the tetraphenyl substitution. This is evidenced by differential changes in the bond length alternation and dihedral angles among the phenylene units of the nanoring. After an initial photoexcitation, the exciton-vibrational dynamics induces an efficient exciton migration from the region close to the tetraphenyl substitution to the rest of the nanoring. Consequently, a more localized exciton self-trapping is achieved due to substitution.

Our results encourage and guide the study of future chemically modified carbon nanorings toward tuning their optoelectronic properties. Specifically, considered type of substitution increases the efficiency of nonradiative relaxation of the nanoring. Moreover, control over localization of the exciton self-trapping relative to the substitution is a valuable property for designing efficient energy-transfer systems.

Notes

The authors declare no competing financial interest. The Non-adiabatic EXcited state molecular dynamics (NEXMD) program code, license, and documentation may be accessed at https://github.com/lanl/NEXMD.

Acknowledgements

This work was partially supported by CONICET, UNQ, ANPCyT (PICT-2018-2360). S. T. gratefully acknowledge support from the Chemical Sciences, Geosciences, and Bio-Sciences Division, Office of Basic Energy Sciences, Office of Science, US Department of Energy (DOE), through award DE-SC0019484 and under Triad National Security, LLC ("Triad") contract grant # 89233218CNA000001 (FWP: LANLE3T1). The work at Los Alamos National Laboratory (LANL) was performed in part at the Center for Center for Integrated Nanotechnologies (CINT), a U.S. Department of Energy, Office of Science User

Facility. This research used resources provided by the LANL Institutional Computing Program.

BIBLIOGRAPHY

1 R. Jasti, J. Bhattacharjee, J. Neaton and C. Bertozzi, Synthesis, Characterization, and Theory of [9]-, [12]-, and [18]Cycloparaphenylene: Carbon Nanohoop Structures, *J. Am. Chem. Soc.*, 2008, **130**, 17646–17647.

2 S. Yamago, Y. Watanabe and T. Iwamoto, Synthesis of [8]Cycloparaphenylene from a Square-Shaped Tetranuclear Platinum Complex, *Angew. Chem., Int. Ed.*, 2010, **49**, 757.

3 N. Kubota, Y. Segawa and K. Itami, n6-Cycloparaphenylene transition metal complexes: Synthesis, structure, photophysical properties, and application to the selective monofunctionalization of cycloparaphenylenes, *J. Am. Chem. Soc.*, 2015, **137**, 1356–1361.

4 Y. Segawa, H. Omachi and K. Itami, Theoretical Studies on the Structures and Strain Energies of Cycloparaphenylenes, *Org. Lett.*, 2010, **12**, 2262.

5 N. Oldani, S. K. Doorn, S. Tretiak and S. Fernandez-Alberti, Photoinduced dynamics in cycloparaphenylenes: Planarization, electron-phonon coupling, localization and intra-ring migration of the electronic excitation, *Phys. Chem. Chem. Phys.*, 2017, **19**, 30914–30924.

6 J. Kim, R. Kishi, E. Kayahara, W. Kim, S. Yamago, M. Nakano and D. Kim, Ultrafast Exciton Self-Trapping and Delocalization in Cycloparaphenylenes: The Role of Excited-State Symmetry in Electron-Vibrational Coupling, *Angew. Chemie*, 2020, **132**, 17137–17144.

7 Y. Segawa, A. Yagi, H. Ito and K. Itami, A Theoretical Study on the Strain Energy of Carbon Nanobelts, *Org. Lett.*, 2016, **18**, 1430–1433.

8 L. Adamska, I. Nayyar, H. Chen, A. Swan, N. Oldani, S. Fernandez-Alberti, M. Golder, R. Jasti, S. Doorn and S. Tretiak, Self-trapping of excitons , violation of Condon approximation and efficient fluorescence in conjugated cycloparaphenylenes ., *Nano Lett.*, 2014, **14**, 6539–6546.

9 Y. Segawa, A. Fukazawa, S. Matsuura, H. Omachi, S. Yamaguchi, S. Irle and K. Itami, Combined experimental and theoretical studies on the photophysical properties of cycloparaphenylenes, *Org. Biomol. Chem.*, 2012, **10**, 5979–5984.

10 E. Darzi, T. Sisto and R. Jasti, Selective Syntheses of [7]–[12]Cycloparaphenylenes Using Orthogonal Suzuki–Miyaura Cross-Coupling Reactions, *J. Org. chem.*, 2012, **77**, 6624–6628.

11 T. Nishihara, Y. Segawa, K. Itami and Y. Kanemitsu, Excited states in

cycloparaphenylenes: Dependence of optical properties on ring length, *J. Phys. Chem. Lett.*, 2012, **3**, 3125–3128.

12 M. Fujitsuka, D. Cho, T. Iwamoto, S. Yamago and T. Majima, Size-dependent fluorescence properties of [n]cycloparaphenylenes (n = 8–13), hoop-shaped π-conjugated molecules, *Phys. Chem. Chem. Phys.*, 2012, **14**, 14585–14588.

13 T. Iwamoto, Y. Watanabe, Y.-I. Sakamoto, T. Suzuki and S. Yamago, Selective and Random Syntheses of [n]Cycloparaphenylenes (n = 8–13) and Size Dependence of Their Electronic Properties, *J. Am. Chem. Soc.*, 2011, **133**, 8354.

14 D. Sundholm, S. Taubert and F. Pinchierri, Calculation of absorption and emission spectra of [n]cycloparaphenylenes: the reason for the large Stokes shift, *Phys. Chem. Chem. Phys.*, 2010, **12**, 2751–2757.

15 B. Wong, Optoelectronic Properties of Carbon Nanorings: Excitonic Effects from Time-Dependent Density Functional Theory, *J. Phys. Chem. C*, 2009, **113**, 21921.

16 C. Camacho, T. Niehaus, K. Itami and S. Irle, Origin of the size-dependent fluorescence blueshift in [n]cycloparaphenylenes, *Chem. Sci.*, 2013, **4**, 187–195.

17 P. Li, T. Sisto, E. Darzi and R. Jasti, The Effects of Cyclic Conjugation and Bending on the Optoelectronic Properties of Paraphenylenes, *Org. Lett.*, 2013, **16**, 182–185.

18 E. R. Darzi and R. Jasti, The dynamic, size-dependent properties of [5]–[12]cycloparaphenylenes, *Chem. Soc. Rev.*, 2015, **44**, 6401–6410.

19 E. J. Leonhardt and R. Jasti, Emerging applications of carbon nanohoops, *Nat. Rev. Chem.*, 2019, **3**, 672–686.

20 S. Lewis, Cycloparaphenylenes and related nanohoops, *Chem. Soc. Rev.*, 2015, **44**, 2221–2304.

21 A. Yagi, Y. Segawa and K. Itami, Synthesis and Properties of [9]Cyclo-1,4-naphthylene: A π-Extended Carbon Nanoring, *J. Am. Chem. Soc.*, 2012, **134**, 2962.

22 B. Rodríguez-Hernández, N. Oldani, A. Martínez-Mesa, L. Uranga-Piña, S. Tretiak and S. Fernandez-Alberti, Photoexcited energy relaxation and vibronic couplings in π-conjugated carbon nanorings, *Phys. Chem. Chem. Phys.*, 2020, **22**, 15321–15332.

23 H. Omachi, T. Nakayama, E. Takahashi, Y. Segawa and K. Itami, Initiation of carbon nanotube growth by well-defined carbon nanorings, *Nat. Chem.*, 2013, **5**, 572–576.

24 E. Hirst, F. Wang and J. Jasti, Theoretical Analysis of [5.7]nCyclacenes: Closed-Shell Cyclacene Isomers, *Org. Lett.*, 2011, **13**, 6220–6223.

25 T. Iwamoto, E. Kayahara, N. Yasuda, T. Suzuki and S. Yamago, Synthesis, Characterization, and Properties of [4]Cyclo-2,7-pyrenylene: Effects of Cyclic Structure on the Electronic Properties of Pyrene Oligomers, *Angew. Chemie*, 2014,

126, 6548–6552.

26 R. Franklin-Mergarejo, T. Nelson, S. Tretiak and S. Fernandez-Alberti, Phonon bottleneck and long-lived excited states in π-conjugated pyrene hoop, *Phys. Chem. Chem. Phys.*, 2017, **19**, 9478–9484.

27 H. Omachi, Y. Segawa and K. Itami, Synthesis and racemization process of chiral carbon nanorings: A step toward the chemical synthesis of chiral carbon nanotubes, *Org. Lett.*, 2011, **13**, 2480–2483.

28 R. Franklin-Mergarejo, D. O. Alvarez, S. Tretiak and S. Fernandez-Alberti, Carbon nanorings with inserted acenes: Breaking symmetry in excited state dynamics, *Sci. Rep.*, , DOI:10.1038/srep31253.

29 B. M. Wong and J. W. Lee, Anomalous Optoelectronic Properties of Chiral Carbon Nanorings…and One Ring to Rule Them All(23), *J. Phys. Chem. Lett.*, 2011, **2**, 2702–2706.

30 G. Povie, Y. Segawa, T. Nishihara1, Y. Miyauchi and K. Itami, Synthesis of a carbon nanobelt, *Science (80-.).*, 2017, **356**, 172–175.

31 Y. Li, H. Kono, T. Maekawa, Y. Segawa, A. Yagi and K. Itami, Chemical Synthesis of Carbon Nanorings and Nanobelts, *Accounts Mater. Res.*, 2021, **2**, 681–691.

32 K. Y. Cheung, K. Watanabe, Y. Segawa and K. Itami, Synthesis of a zigzag carbon nanobelt, *Nat. Chem.*, 2021, **13**, 255–259.

33 K. Matsui, Y. Segawa, T. Namikawa, K. Kamada and K. Itami, Synthesis and properties of all-benzene carbon nanocages: a junction unit of branched carbon nanotubes, *Chem. Sci.*, 2013, **4**, 84.

34 Y. Segawa, M. Kuwayama, Y. Hijikata, M. Fushimi, T. Nishihara, J. Pirillo, J. Shirasaki, N. Kubota and K. Itami, Topological molecular nanocarbons: All-benzene catenane and trefoil knot, *Science (80-.).*, 2019, **365**, 272–276.

35 S. Canola, C. Graham, Á. J. Pérez-Jiménez, J. C. Sancho-García and F. Negri, Charge transport parameters for carbon based nanohoops and donor-acceptor derivatives, *Phys. Chem. Chem. Phys.*, 2019, **21**, 2057–2068.

36 M. Barbatti, G. Granucci, M. Persico, M. Ruckenbauer, M. Vazdar, M. Eckert-Maksić and H. Lischka, The on-the-fly surface-hopping program system Newton-X: Application to ab initio simulation of the nonadiabatic photodynamics of benchmark systems, *J. Photochem. Photobiol. A Chem.*, 2007, **190**, 228–240.

37 M. Barbatti, M. Ruckenbauer, F. Plasser, J. Pittner, G. Granucci, M. Persico and H. Lischka, Newton-X: A surface-hopping program for nonadiabatic molecular dynamics, *Wiley Interdiscip. Rev. Comput. Mol. Sci.*, 2014, **4**, 26–33.

38 M. Richter, P. Marquetand, J. González-Vázquez, I. Sola and L. González, SHARC: Ab initio molecular dynamics with surface hopping in the adiabatic representation

including arbitrary couplings, *J. Chem. Theory Comput.*, 2011, **7**, 1253–1258.

39 S. Mai, P. Marquetand and L. González, Nonadiabatic dynamics: The SHARC approach, *Wiley Interdiscip. Rev. Comput. Mol. Sci.*, 2018, **8**, 1–23.

40 A. V. Akimov and O. V. Prezhdo, The PYXAID program for non-adiabatic molecular dynamics in condensed matter systemsmics in condensed matter systems, *J. Chem. Theory Comput.*, 2013, **9**, 4959–4972.

41 A. V. Akimov and O. V. Prezhdo, Advanced capabilities of the PYXAID program: Integration schemes, decoherence effects, multiexcitonic states, and field-matter interaction, *J. Chem. Theory Comput.*, 2014, **10**, 789–804.

42 J. Quenneville and T. J. Martı, Ab Initio Multiple Spawning : Photochemistry from First Principles Quantum Molecular.

43 B. G. Levine, J. D. Coe, A. M. Virshup and T. J. Martínez, Implementation of ab initio multiple spawning in the Molpro quantum chemistry package, *Chem. Phys.*, 2008, **347**, 3–16.

44 W. Malone, B. Nebgen, A. White, Y. Zhang, H. Song, J. Bjorgaard, A. Sifain, B. Rodriguez-Hernan, V. Freixas, S. Fernandez-Alberti, A. Roitberg, T. Nelson and S. Tretiak, NEXMD Software Package for Non-adiabatic Excited State Molecular Dynamics Simulations, *J. Chem. Theory Comput.*, 2020, **16**, 5771–5783.

45 A. E. Sifain, J. A. Bjorgaard, T. R. Nelson, B. T. Nebgen, A. J. White, B. J. Gifford, D. W. Gao, O. V. Prezhdo, S. Fernandez-Alberti, A. E. Roitberg and S. Tretiak, Photoexcited Nonadiabatic Dynamics of Solvated Push–Pull π-Conjugated Oligomers with the NEXMD Software, *J. Chem. Theory Comput.*, 2018, **14**, 3955–3966.

46 R. Crespo-Otero and M. Barbatti, Recent Advances and Perspectives on Nonadiabatic Mixed Quantum-Classical Dynamics, *Chem. Rev.*, 2018, **118**, 7026–7068.

47 J. P. Zobel and L. González, The Quest to Simulate Excited-State Dynamics of Transition Metal Complexes, *JACS Au*, 2021, **1**, 1116–1140.

48 A. J. Atkins and L. González, Trajectory Surface-Hopping Dynamics Including Intersystem Crossing in [Ru(bpy)3]2+, *J. Phys. Chem. Lett.*, 2017, **8**, 3840–3845.

49 I. Schapiro, D. Roca-Sanjuán, R. Lindh and M. Olivucci, A surface hopping algorithm for nonadiabatic minimum energy path calculations, *J. Comput. Chem.*, 2015, **36**, 312–320.

50 F. Talotta, S. Morisset, N. Rougeau, D. Lauvergnat and F. Agostini, Internal Conversion and Intersystem Crossing with the Exact Factorization, *J. Chem. Theory Comput.*, 2020, **16**, 4833–4848.

51 D. Avagliano, M. Bonfanti, M. Garavelli and L. González, QM/MM Nonadiabatic

Dynamics: The SHARC/COBRAMM Approach, *J. Chem. Theory Comput.*, 2021, **17**, 4639–4647.

52 H. Song, Y. Nam, D. Keefer, M. Garavelli, S. Mukamel and S. Tretiak, Nonadiabatic Molecular Dynamics Study of the Relaxation Pathways of Photoexcited Cyclooctatetraene, *J. Phys. Chem. Lett.*, 2021, **12**, 5716–5722.

53 T. R. Nelson, A. J. White, J. A. Bjorgaard, A. E. Sifain, Y. Zhang, B. Nebgen, S. Fernandez-alberti, D. Mozyrsky, A. E. Roitberg and S. Tretiak, Non-adiabatic Excited-State Molecular Dynamics : Theory and Applications for Modeling Photophysics in Extended Molecular Materials, *Chem. Rev.*, 2020, **120**, 2215–2287.

54 A. Sisto, C. Stross, M. W. Van Der Kamp, M. O'Connor, S. McIntosh-Smith, G. T. Johnson, E. G. Hohenstein, F. R. Manby, D. R. Glowacki and T. J. Martinez, Atomistic non-adiabatic dynamics of the LH2 complex with a GPU-accelerated: Ab initio exciton model, *Phys. Chem. Chem. Phys.*, 2017, **19**, 14924–14936.

55 B. F. E. Curchod and T. J. Martínez, Ab Initio Nonadiabatic Quantum Molecular Dynamics, *Chem. Rev.*, 2018, **118**, 3305–3336.

56 M. Ruckenbauer, M. Barbatti, T. Müller and H. Lischka, Nonadiabatic photodynamics of a retinal model in polar and nonpolar environment, *J. Phys. Chem. A*, 2013, **117**, 2790–2799.

57 D. Nachtigallová, T. Zelený, M. Ruckenbauer, T. Müller, M. Barbatti, P. Hobza and H. Lischka, Does stacking restrain the photodynamics of individual nucleobases-, *J. Am. Chem. Soc.*, 2010, **132**, 8261–8263.

58 C. E. Crespo-Hernández, L. Martínez-Fernández, C. Rauer, C. Reichardt, S. Mai, M. Pollum, P. Marquetand, L. González and I. Corral, Electronic and Structural Elements That Regulate the Excited-State Dynamics in Purine Nucleobase Derivatives, *J. Am. Chem. Soc.*, 2015, **137**, 4368–4381.

59 J. F. Galindo, E. Atas, A. Altan, D. G. Kuroda, S. Fernandez-Alberti, S. Tretiak, A. E. Roitberg and V. D. Kleiman, Dynamics of Energy Transfer in a Conjugated Dendrimer Driven by Ultrafast Localization of Excitations, *J. Am. Chem. Soc.*, 2015, **137**, 11637–11644.

60 J. Liu and W. Thiel, An efficient implementation of semiempirical quantum-chemical orthogonalization-corrected methods for excited-state dynamics, *J. Chem. Phys.*, , DOI:10.1063/1.5022466.

61 B. Smith and A. V. Akimov, Modeling nonadiabatic dynamics in condensed matter materials: Some recent advances and applications, *J. Phys. Condens. Matter*, , DOI:10.1088/1361-648X/ab5246.

62 L. Stojanović, S. G. Aziz, R. H. Hilal, F. Plasser, T. A. Niehaus and M. Barbatti, Nonadiabatic Dynamics of Cycloparaphenylenes with TD-DFTB Surface Hopping, *J. Chem. Theory Comput.*, 2017, **13**, 5846–5860.

63 B. Rodríguez-Hernández, D. Ondarse-Álvarez, N. Oldani, A. Martínez-Mesa, L. Uranga-Piña, S. Tretiak and S. Fernández-Alberti, Modification of Optical Properties and Excited-State Dynamics by Linearizing Cyclic Paraphenylene Chromophores, *J. Phys. Chem. C*, 2018, **122**, 16639–16648.

64 V. M. Freixas, N. Oldani, R. Franklin-Mergarejo, S. Tretiak and S. Fernandez-Alberti, Electronic Energy Relaxation in a Photoexcited Fully Fused Edge-Sharing Carbon Nanobelt, *J. Phys. Chem. Lett.*, 2020, **11**, 4711–4719.

65 B. Rodríguez-Hernández, T. Nelson, N. Oldani, A. Martínez-Mesa, L. Uranga-Piña, Y. Segawa, S. Tretiak, K. Itami and S. Fernandez-Alberti, Exciton Spatial Dynamics and Self-Trapping in Carbon Nanocages, *J. Phys. Chem. Lett.*, 2021, **12**, 224–231.

66 T. Sisto, X. Tian and R. Jasti, Synthesis of Tetraphenyl-Substituted [12]Cycloparaphenylene: Toward a Rationally Designed Ultrashort Carbon Nanotube, *J. Org. Chem.*, 2012, **77**, 5857.

67 J. C. Tully, Molecular dynamics with electronic transitions, *J. Chem Phys.*, 1990, **93**, 1061–1071.

68 S. Hammes-schiffer and J. C. Tully, Proton transfer in solution : Molecular dynamics with quantum transitions, *J. Chem Phys.*, 1994, **101**, 4657–4667.

69 T. Nelson, S. Fernandez-Alberti, A. E. Roitberg and S. Tretiak, Nonadiabatic Excited State Molecular Dynamics: Modeling Photophysics in Organic Conjugated Materials, *Acc. Chem. Res.*, 2014, **47**, 1155–1164.

70 S. Tretiak, C. M. Isborn, A. M. N. Niklasson and M. Challacombe, Representation independent algorithms for molecular response calculations in time-dependent self-consistent field theories, *J. Chem. Phys.*, 2009, **130**, 054111–054127.

71 R. J. Bell, P. Dean and D. C. Hibbins-Butler, Localization of normal modes i n vitreous silica , germania and beryllium fluoride, *J. Phys. C Solid St. Phys*, 1970, **3**, 2111–2118.

72 S. N. Taraskin and S. R. Elliott, Anharmonicity and localization of atomic vibrations in vitreous silica, *Phys. Rev. B*, 1999, **59**, 8572–8585.

73 L. Alfonso Hernandez, T. Nelson, M. F. Gelin, J. M. Lupton, S. Tretiak and S. Fernandez-Alberti, Interference of Interchromophoric Energy-Transfer Pathways in π-Conjugated Macrocycles, *J. Phys. Chem. Lett.*, 2016, **7**, 4936–4944.

74 M. A. Soler, A. Bastida, M. H. Farag, J. Zúñiga and A. Requena, A method for analyzing the vibrational energy flow in biomolecules in solution., *J. Chem. Phys.*, 2011, **135**, 204106.

75 M. J. S. Dewar, E. G. Zoebisch, E. F. Healy and J. J. P. Stewart, The development and use of quantum-mechanical molecular-models.76.AM1 - A new general purpose quantum-mechanical molecular-model, *J. Am. Chem. Soc.*, 1985, **107**, 3902–3909.

76 T. Nelson, S. Fernandez-alberti, A. E. Roitberg and S. Tretiak, Nonadiabatic Excited-State Molecular Dynamics : Treatment of Electronic Decoherence, *J. Chem. Phys.*, 2013, **138**, 224111.

77 S. Fernandez-Alberti, A. E. Roitberg, T. Nelson and S. Tretiak, Identification of unavoided crossings in nonadiabatic photoexcited dynamics involving multiple electronic states in polyatomic conjugated molecules., *J. Chem. Phys.*, 2012, **137**, 014512.

78 M. Fujitsuka, T. Iwamoto, E. Kayahara, S. Yamago and T. Majima, Enhancement of the quinoidal character for smaller [n]cycloparaphenylenes probed by Raman spectroscopy., *ChemPhysChem*, 2013, **14**, 1570.

79 I. Franco and S. Tretiak, Electron-vibrational dynamics of photoexcited polyfluorenes, *J. Am. Chem. Soc.*, 2004, **126**, 12130–12140.

80 J. Liu, L. Adamska, S. K. Doorn and S. Tretiak, Singlet and triplet excitons and charge polarons in cycloparaphenylenes: a density functional theory study, *Phys. Chem. Chem. Phys.*, 2015, **17**, 14613–14622.

81 M. Soler, A. Roitberg, T. Nelson, S. Tretiak and S. Fernandez-Alberti, Analysis of state-specific vibrations coupled to the unidirectional energy transfer in conjugated dendrimers., *J. Phys. Chem. A*, 2012, **116**, 9802–10.